ADVANCED FUNCTIONAL MATERIALS
www.afm-journal.de

Solvent-Independent 3D Printing of Organogels

*Mariia A. Kuzina, Maxi Hoffmann, Nikolaj K. Mandsberg, Carmen M. Domínguez, Christof M. Niemeyer, Manfred Wilhelm, and Pavel A. Levkin**

Organogels are polymer networks extended by a liquid organic phase, offering a wide range of properties due to the many combinations of polymer networks, solvents, and shapes achievable through 3D printing. However, current printing methods limit solvent choice and composition, which in turn limits organogels' properties, applications, and potential for innovation. As a solution, a method for solvent-independent printing of 3D organogel structures is presented. In this method, the printing step is decoupled from the choice of solvent, allowing access to the full spectrum of solvent diversity, thereby significantly expanding the range of achievable properties in organogel structures. With no changes to the polymer network, the 3D geometry, or the printing methodology itself, the choice of solvent alone is shown to have an enormous impact on organogel properties. As demonstrated, it can modulate the thermo-mechanical properties of the organogels, both shifting and extending their thermal stability range to span from -30 to over 100 °C. The choice of solvent can also transition the organogels from highly adhesive to extremely slippery. Finally, the method also improves the surface smoothness of prints. Such advances have potential applications in soft robotics, actuators, and sensors, and represent a versatile approach to expanding the functionality of 3D-printed organogels.

1. Introduction

Organogels constitute a subcategory of gels, created by a three-dimensional supramolecular or covalent polymer network, infused with a liquid organic phase.[1–5] Organogels exhibit a unique wide range of properties that result from the diverse chemical structure of the gelators, the network structure, the properties of the liquid phase, and their intricate interactions.[3,4] Examples of organogels' properties derived directly from the liquid phase include photodegradability,[5] increased working temperature gap for electrically conductive gels,[6–8] promoted growth of nanocrystals and enhanced fluorescence,[9] and boosted mechanical performance, such as their stretchability[10] or notch resistance.[11] Organogels have already shown their potential in various applications, such as anti-adhesive[12] and self-cleaning surfaces,[13] drug carriers,[6,14] sensors,[15] actuators,[16,17] and extraction vessels.[18,19] However, the diverse properties offered by organic solvents are largely untapped due to the limited research on organogels compared to hydrogels.[1]

Current progress in universal and convenient fabrication methods for organogels is mainly limited to films,[20–22] coatings,[23–25] and nanostructured bulk gels.[10,23,26,27] Recently, irradiation through photomasks has been developed to structure organogels and enhance their functionality. This technique has been utilized to create liquid channels and gel photoresists,[5,28] as well as fabricate reversible organogel holograms.[29] The incorporation of 3D-printing into this important class of materials could further expand the range of applications.[30,31] However, there have been only a few published attempts to apply additive manufacturing to fabricate organogels. Zhang et al. demonstrated 3D-printable homogeneously luminescent organogels with complex free-standing architectures, which are not otherwise achievable for flexible perovskite gels.[32] O'Bryan et al. demonstrated a method for 3D-printing of silicon-based structures through self-assembling micro-organogel based block copolymer in mineral oil.[33]

The primary challenge in 3D printing organogels is the incompatibility of many organic solvents with current 3D printing technologies. This problem is particularly pronounced when printing structures with high solvent content, resulting in slow cross-linking and reduced mechanical strength. Consequently,

M. A. Kuzina, N. K. Mandsberg, P. A. Levkin
Karlsruhe Institute of Technology (KIT)
Institute of Biological and Chemical Systems – Functional Molecular Systems (IBCS-FMS)
Kaiserstrasse 12, 76131 Karlsruhe, Germany
E-mail: levkin@kit.edu

M. Hoffmann, M. Wilhelm
Karlsruhe Institute of Technology (KIT)
Institute for Chemical Technology and Polymer Chemistry (ITCP)
Engesserstraße 18, 76131 Karlsruhe, Germany

C. M. Domínguez, C. M. Niemeyer
Karlsruhe Institute of Technology (KIT)
Institute for Biological Interfaces (IBG-1)
Karlsruhe Institute of Technology (KIT)
Hermann-von-Helmholtz Platz 1, 76344 Eggenstein-Leopoldshafen, Germany

The ORCID identification number(s) for the author(s) of this article can be found under https://doi.org/10.1002/adfm.202403694

DOI: 10.1002/adfm.202403694

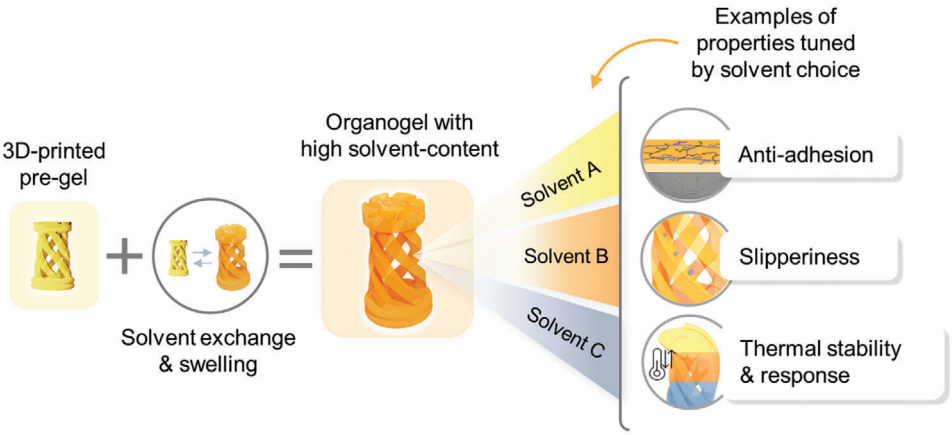

Figure 1. Solvent-independent 3D printing of organogels with preserved control over properties. 3D-printing provides free choice of shape and rapid production, but is limited in the choice of solvent. Printing with a sacrificial solvent and with subsequent swelling in the solvent of interest allows solvent-independent fabrication of 3D organogels with a wide range of functionalities, such as extreme thermal stability and response, and enhanced surface properties.

printing a diverse range of organogels with varying solvent compositions using 3D printing technology remains a challenge. This has limited the exploration of their unique properties when integrated with 3D printing.

Here, we present a universal, convenient, and tunable method to fabricate solvent-independent organogels with high liquid fractions via Digital Light Processing (DLP) 3D printing, and explore their behavior and properties as a function of ink composition, swelling solvents, and complexity of the macroscopic 3D structure (**Figure 1**). The key innovation of our approach is the separation of the swelling and solvent choice from the printing step. This is achieved by initially fabricating swellable 3D-printed organogels, followed by a solvent exchange and a secondary swelling step, enabling high solvent content in a solvent-independent manner. This approach enables us to freely vary the liquid phase and increase solvent content (from 20–30 wt% up to 90 wt%) without compromising printing resolution. The solvent-defined properties of organogels, such as tunable thermal stability and swelling, as well as unique surface wettability and adhesive properties, are investigated in this study. This method enables the fabrication of 3D structures of organogels independent of the swelling solvent and achieving very high solvent content. These developments present new opportunities for utilizing this fascinating class of materials with a wider range of potential functions that rely on the interplay between 3D geometry, polymer network, swelling solvent, and solvent content.

2. Results and Discussion

The method involves printing a base organogel structure using a non-volatile sacrificial mineral oil, then replacing this base solvent with other organic liquids while maintaining the 3D geometry.

Organogels were fabricated using DLP 3D-printing. The ink consisted of lauryl acrylate as a monomer, polypropylene glycol dimethacrylate as a cross-linker, a photoinitiator irgacure 379 (2-dimethylamino-2-(4-methyl-benzyl)−1-(4-morpholin-4-yl-phenyl)butan-1-one), and a biotolerant white paraffin mineral oil as a solvent. The molecular structures and the exact compositions used for printing are presented in Figure S1 (Supporting Information). After printing, the objects were immersed in n-isopropanol for 24 h and subsequently air-dried for 8–12 h. The dried objects were then immersed in various solvents to evaluate the specific effect of each on swelling behavior (**Figure 2A**). The swelling enlarged defined features while retaining their original geometry, both before (Figure 2B) and after swelling (Figure 2C). The 3D-printed organogels can take on various shapes, such as sharp, round, hollow, and twisted, with feature resolution down to the submillimeter scale (Figure 2D). This resolution is similar to the typical feature size achieved for bottom-up DLP 3D printing of hydrogels.[34] Our DLP system's single mirror size was 40 µm, which defines our theoretical maximum resolution. Other DLP systems have reportedly achieved resolutions down to the 1 µm range by focusing of the projected light, leaving room for future improvements.[35,36]

The swelling kinetics varied among new solvents (Figure 2E), with the slowest and fastest equilibration rates observed for 1-decanol and n-octane, respectively. Equilibration for long-chain solvents required several days to a week, while for n-octane, it was achieved in less than 12 h. The Voigt viscoelastic swelling model was used to fit the swelling kinetics, and the resulting fit values were used to calculate the swelling equilibrium size and swelling rate coefficient (see Figure S2, Supporting Information, for the fit values). We also briefly investigated how 3D morphology affects swelling kinetics by comparing the swelling of a bulk cube with a mesh cube, observing how also geometry affects the absorption rate by altering the diffusion length scale (see Figures S3 and S4, Supporting Information).

To further regulate the swelling equilibrium value, the cross-linker content was reduced from 1 to 0.5 mol%, resulting in a larger uptake of the swelling liquid, from 350 ± 5 to 560 ± 15 wt% (Figure 2F, swelling solvent: 1-decanol). This change in swelling behavior corresponds to the Flory-Rehner swelling equilibrium equation, which states that networks with higher cross-linking density exhibit reduced swelling capacity.[37,38] Control over the swelling ratio was also demonstrated by changing the monomer

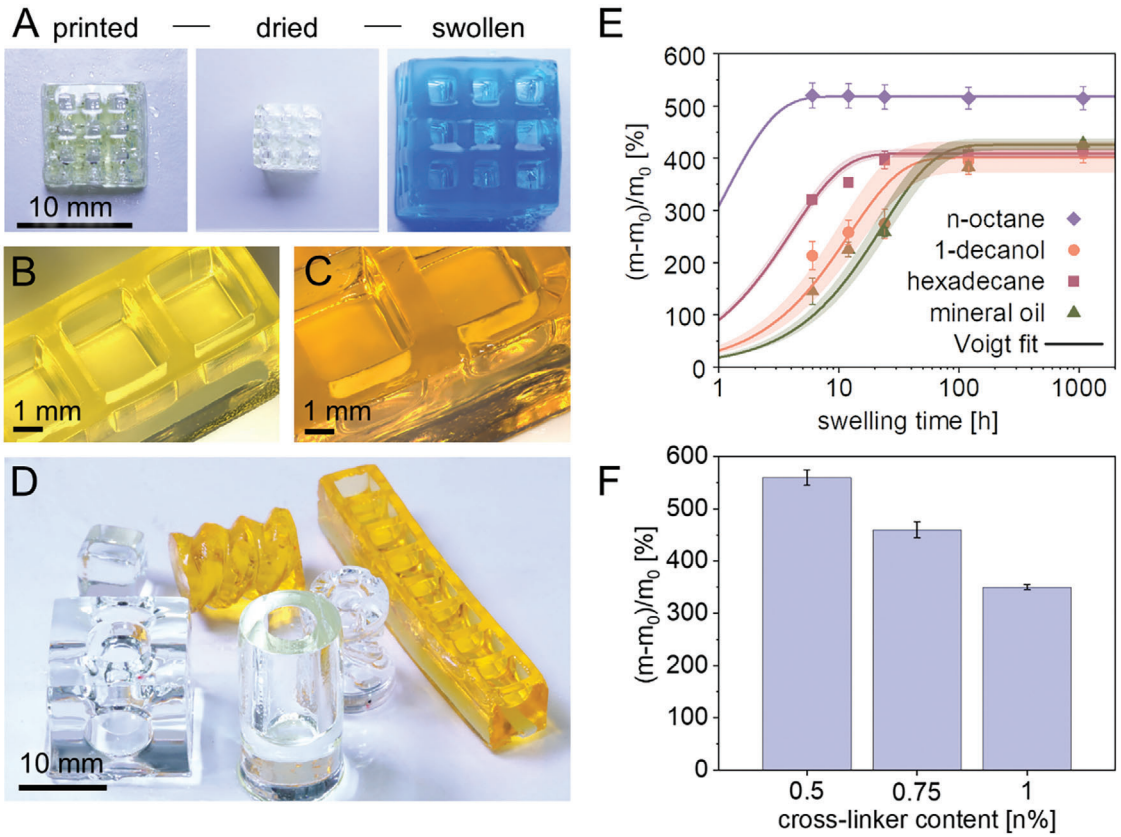

Figure 2. Swelling of 3D-printed organogel. A) Organogel as printed (left), after solvent replacement by isopropanol and drying in air (middle), and after swelling in toluene dyed with Oil Blue O (right). The original 3D structure of the organogel B) remains intact after solvent exchange, drying, and swelling C,D). The ink and polymer components are detailed in Figure S1A (Supporting Information). E) Swelling kinetics of the organogel LA80CL1 over 1080 h (45 days) of swelling in various solvents (n = 3, sample replicates). Curves are fitted based on the Voigt viscoelastic model and plotted with uncertainties. F) Mean swelling values after 24 h in 1-decanol for inks with cross-linker content ranging from 0.5 to 1 mol.% relative to the monomer (ink names, from left to right: LA80CL0.5, LA80CL0.75, LA80CL1). (n = 3, sample replicates).

content in the original ink (Figure S5, Supporting Information). This shows the importance of the solvent-to-monomer weight ratio in the printing ink being at least 20:80. A flexible and less dense polymer network was achieved with 20 wt% of organic solvent in the printing ink, resulting in a higher swelling ratio for the organogel after printing. However, increasing the solvent amount to over 50 wt% had a negative impact on ink reactivity and resulted in printing failure of complex structures.

One concern regarding the fabricated organogels is their stability. Our methodology uses covalently cross-linked networks, which inherently minimizes potential degradation risks during both printing and post-processing phases, including swelling. This stability is evident in the 45-day swelling experiments (Figure 2E). Gel swelling stabilized after 10–100 h, depending on the solvent, and remained unchanged thereafter, indicating no significant degradation over the testing period. Furthermore, previous explorations into ultraviolet (UV) degradation of covalently crosslinked methacrylate have shown minimal impact at wavelengths above 320 nm,[39,40] confirming the stability of these materials under the 385 nm wavelength used in our DLP 3D printing process. For the swollen gels, the degree of UV degradation depends on the swelling degree, monomer, crosslinker, and solvent.[5] Degradation requires low network density, high solvent content, and a solvent that does not effectively absorb the UV light. Overall, it can be inferred that there is minimal to no degradation for our non-swollen gels, while for swollen gels, the extent of degradation may vary. These considerations are pertinent to the organogels' durability, which is crucial to their functional integrity across a wide range of applications.

The properties of swollen organogels may be influenced by whether the solvent is infused post-printing (our method) or integrated during the printing process. However, the extent of this influence is likely dependent on the specific network-solvent combination used. Similar organogel properties may be achieved by both pathways with non-interacting solvents, defined as those that do not alter the polymer network architecture. Conversely, using an interacting sacrificial solvent could intentionally modify the network architecture, thereby affecting the properties of the resulting organogel.

Interestingly, lauryl acrylate-based organogels printed using mineral oil as a solvent exhibit strong wet and solid adhesion (**Figure 3**). This effect can be reversed by replacing the initial solvent (mineral oil) with a low surface tension solvent.[41] To demonstrate the effect of swelling on the surface of the organogel, flat organogel structures (20 × 10 × 3 mm^3) were printed using mineral oil as a solvent. These structures were

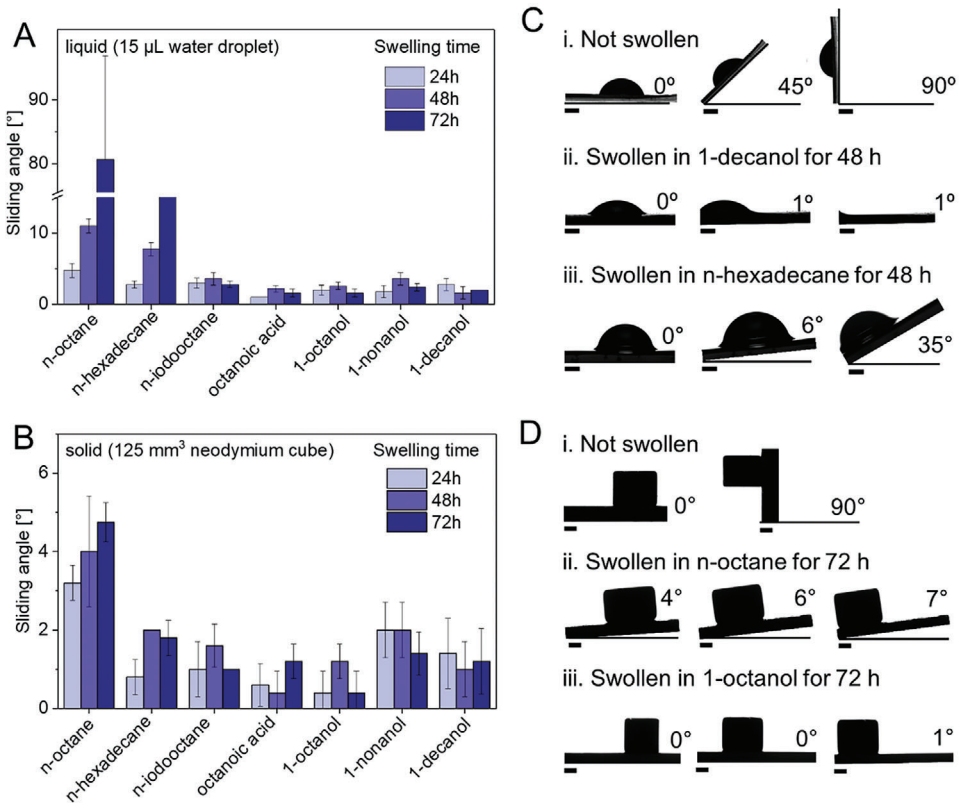

Figure 3. Tuning organogel properties from high adhesion to extreme slipperiness. The organogels exhibit tunable surface interactions with both liquids and solids. A) Sliding angles for 15 µL water drops on organogels swollen in various solvents for different durations (n = 3). B) Neodymium cube (125 mm^3) sliding angles on similarly prepared organogels. Visual comparisons: C) A water drop adheres to an unswollen organogel i), but slides off organogels swollen in 1-decanol ii), and n-hexadecane iii). D) A neodymium cube sticks to an unswollen organogel i) but slides off those swollen in n-octane ii) and 1-octanol iii), at angles of 4° and 1°, respectively. Ink composition: LA80CL1. Scale bar: 1 mm. (n = 3).

then swollen for 24, 48, and 72 h in various low surface tension solvents. To characterize wet and solid adhesion, sliding angle measurements were performed using 15 µL of water as a liquid (Figure 3A,C) and a 125 mm^3 (0.91 g) neodymium cube (Figure 3B,D). A droplet shape analyzer platform was tilted from a horizontal to a vertical orientation at a rate of 1 $°s^{-1}$, while the recording the position of the drop or cube. The sliding angle was determined as the moment the position of the water droplet or a cube changed during tilting.

The non-swollen organogel demonstrated full adhesiveness to both liquid (Figure 3C-i) and solid (Figure 3D-i), i.e., no sliding was observed when the sample was turned up to 90 °C and then back down to 0 °C. This behavior is attributed to the known adhesive properties of weakly cross-linked elastomers based on lauryl acrylate.[40,41] To induce swelling, we chose hydrophobic solvents with different functional groups and chain lengths; including aliphatic hydrocarbons with varying chain lengths and boiling points (n-octane, n-hexadecane, 1-iodooctane), hydrophobic alcohols with varying aliphatic chain length (1-octanol, 1-nonanol, 1-decanol) and 1-nonanoic acid as a fatty acid. All of the swollen gels exhibited liquid and solid slippery behavior, with some even showing full loss of adhesion, resulting in near-zero sliding angles. It is worth noting that the degree of slipperiness increased from aliphatic hydrocarbons to hydrophobic solvents with additional functional groups. Based on the average sliding angle for all swelling times (24, 48, and 72 h), the best combination of liquid and solid adhesion was demonstrated by 1-octanoic acid and 1-octanol. Since shorter swelling times did not significantly alter gel slipperiness (see Figure 3A,B), it can be assumed that the solvent lubrication layer on the surface has a greater impact on anti-adhesion than the expansion of the polymer network during swelling. The gel retained its liquid lubrication level for more than 10 cycles and could easily be restored by gently pressing or briefly dipping it in a reservoir with the swelling solvent.

We further explored how surface morphology may influence this transition from adherent to slippery behavior in organogels before and after swelling. Using digital optical microscopy and laser profilometry, we analyzed the surface and cross-section of these gels, revealing a square pattern with a 40 µm period and a depth of several µm (**Figure** 4A–C). This pattern originates from the pixel-based curing of each layer in the DMD printing, with its period being determined by mirror size and its depth determined by the layer thickness, curing time, and intensity of the light source. These surface roughness artefacts also limit the transparency of the gels. However, post-swelling characterization (Figure 4D–F) revealed a significant improvement in surface smoothness, decreasing roughness from ≈5.4 µm to less than 1 µm, thanks to solvent-induced network expansion and surface lubrication (Figure 4B,E). Consequently, the transparency of the gels in the visible spectrum also increased significantly, with the

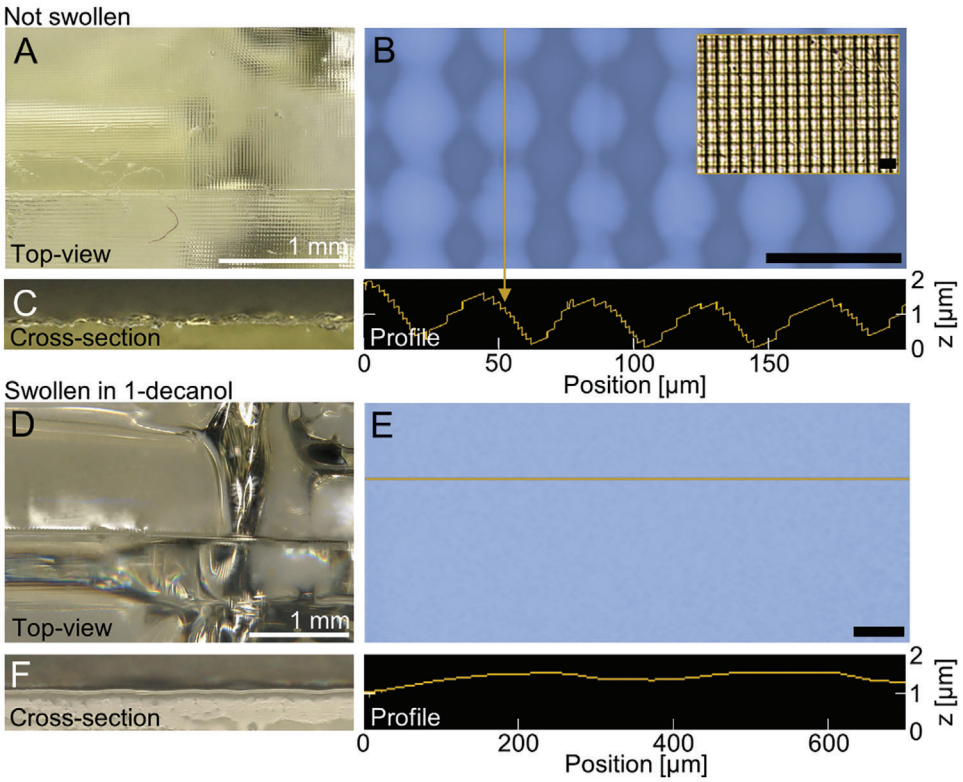

Figure 4. Surface morphology of 3D-printed organogels before and after swelling in 1-Decanol. Initial roughness characterized by a square pattern of 40 µm^2 A,C) reflects the DMD digital mirror size of the printer, with several micrometers in depth (B). D,E) After swelling, surfaces become smooth, E) erasing the pre-swelling pattern. C,F) Cross-sectional views show these changes after a perpendicular cut. Black scale bars: 50 µm.

maximum absorbance dropping from 0.41 to 0.03 a.u. in the 400–700 nm range (spectra in Figure S6, Supporting Information). These findings align with Zhang et al.'s research on the enhancement of transparency in organogels induced by swelling.[41] This demonstrates the potential of swelling as a post-processing technique to improve transparency and reduce printing artefacts in DLP 3D-printed viscoelastic materials.

The impact of solvent on organogel properties is often underappreciated. Here, we demonstrate that the mechanical properties and temperature stability of a 3D-printed organogel can be precisely adjusted by swelling it in different solvents, resulting in tailored thermo-responsive behavior. This phenomenon was characterized using temperature sweep rheometry, as shown in **Figure 5**. Rotational rheometry was chosen as a method to investigate mechanical behavior of the non-swollen versus swollen organogels because it showed to be most suitable setup, which is also traditionally applied for highly swollen, slippery gels,[42–44] whereas the compression and tensile tests did not allow for a proper fixation of the samples and therefore lacked reproducibility. Upon cooling below ≈0 °C, the non-swollen organogel was gradually hardened and lost its flexibility, as indicated by the rising storage and loss moduli (Figure 5A). When swollen in n-hexadecane, the organogel instead exhibited a rapid thermo-responsive switch from soft viscoelastic to stiff behavior at the solvent's melting point, T_m = 18 °C[45] (Figure 5B). Similarly, when swollen in a mineral oil with a lower melting point (T_m ≈ −18 °C), the same organogel, still with the same polymer network, retained its flexibility all the way down to −15 °C with a similarly rapid hardening behavior when approaching the melting point of this solvent (Figure 5C), thus significantly extending the stable temperature range. The tested solvents showed various degrees of flexibility preservation, with the lowest limit observed for the organogel swollen with butyl disulfide (T_m = −94 °C), which remained stable down to ≈−28 °C (Figure 5D). In this case, the stiffening temperature was higher than the melting point of the solvent, which we attribute to the fast evaporation of butyl-disulfide and subsequent hardening of the organogel surface due the solvent deficiency. It is noteworthy that the stiffening of gels can be reversed by subsequent heating, and this stiffening-softening cycle can be repeated without the degradation of the mechanical stability. This was demonstrated by the temperature ramp cycle for the n-hexadecane-swollen organogel (Figure 5E).

The mechanical properties of swollen organogels were stable across a wide temperature range – not just at low temperatures. Rheological testing from 25 to 100 °C on both non-swollen organogels and those swollen in hexadecane for 24 h, showed that while the non-swollen gel's loss modulus varied throughout the heating range (Figure 5G), the swollen organogel maintained stable storage and loss moduli up to 100 °C (Figure 5H). This indicates that organogels with high solvent content can have their mechanical properties, such as reversible stiffening- softening, finely adjusted for stability at both low and high temperatures through swelling. The tuning of thermo-mechanical properties

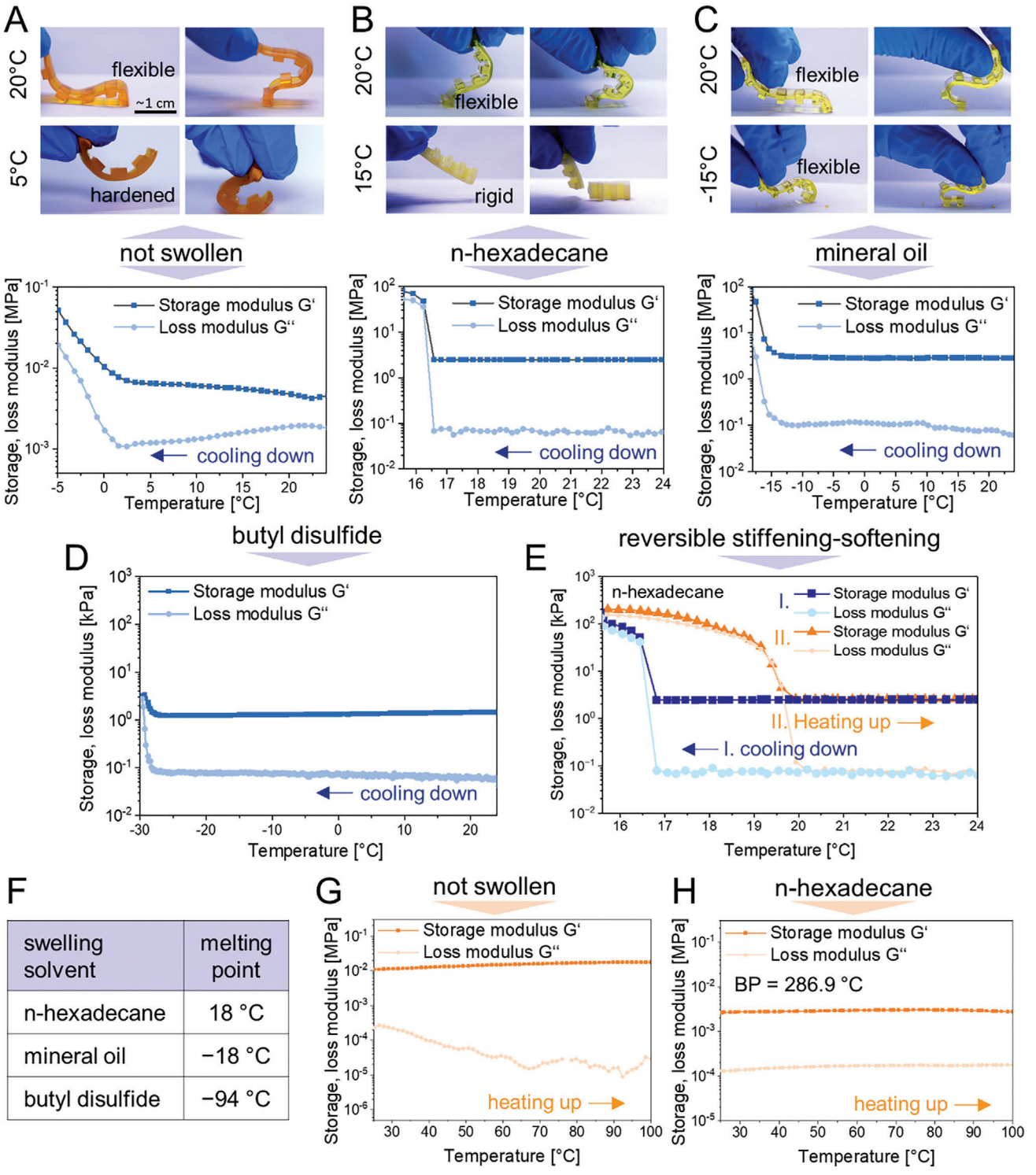

swelling solvent	melting point
n-hexadecane	18 °C
mineral oil	−18 °C
butyl disulfide	−94 °C

Figure 5. Tuning the organogel thermal-mechanical transition: Effects of swelling and solvent selection. Illustrations of the cooling-caused changes to flexibility and temperature-sweep-rheology plots for A) a non-swollen organogel and for an organogel swollen in B) n-hexadecane, C) mineral oil, and D) butyl disulfide. E) Reversible stiffening-softening for the n-hexadecane-swollen organogel demonstrated in a cooling-heating cycle. F) Melting points of the swelling solvents responsible for tuning the range of organogel thermal stability. The illustration of heating-caused changes in thermal stability for G) non-swollen and H) swollen in n-hexadecane organogel. Ink composition for all samples: LA80CL1. All swelling times were 72 h.

is just another example of the powerful influence of solvent selection.

The scalability, reproducibility, and compatibility of the proposed method are pegged to those of typical DLP 3D photopolymerization. We note that the incorporation of volatile solvents into organogels can pose significant challenges for consistent reproduction due to the evaporative component, which can alter printing conditions over time and space. However, our approach can effectively circumvent these issues by utilizing a non-volatile sacrificial solvent, such as mineral oil, during printing and introducing a volatile solvent post-printing, ensuring uniform results across different production scales.

3. Conclusion

We demonstrate a method for creating 3D organogel structures with flexible solvent choice and up to 90% solvent content. By printing with a standardized sacrificial solvent, the method decouples solvent selection from the printing step, addressing the need for a universal, tunable, and solvent-independent method for fabricating complex-shaped organogels. This substantially broadens access to the large spectrum of solvent diversity. Most importantly, we discover an immense impact of solvent choice on organogel properties, showing that a single polymer network can undergo significant, even qualitative, changes simply by infusing it with different solvents.

For instance, we transformed a single polymer network from highly adhesive to completely slippery by swelling it with hydrophobic solvents like medium-chain alcohols, toluene, and oils. Furthermore, swelling in solvents with different melting points modified the thermo-mechanical behavior, extending the thermal stability low temperature (down to −30 °C) and high temperature (up to 100 °C) ranges and enabling reversible hardening-softening cycles with varying solvent-tuned transition temperatures. The organogels' tunable properties combined with additive manufacturing methods, offer new opportunities for their applications in extraction processes, soft robotics, and smart multi-responsive polymers.

Optimization of the 3D manufacturing process for organogels based on a new polymer network is still needed. However, the solvent-independent 3D printing method reduces the optimization problem by one dimension. Previously, exploring all combinations of 100 networks and solvents would have required 10000 distinct protocols. Now, only 100 protocols are needed, improving the efficiency of exploring various combinations. The method also allows for the prefabrication of standard geometries for later infusion with property-modifying solvents, optimizing storage and minimizing waste through more accurate demand forecasting. Noteworthy, this infusion can include solvents that are completely incompatible with 3D printing or highly dangerous/toxic, thereby unlocking the option to create novel 3D organogel structures with unusual properties. Finally, this solvent-derived functionality concept extends to other 3D printing techniques, like two-photon polymerization and stereolithography, offering a versatile method for producing organogels with customizable properties. This innovation is especially relevant for applications beyond the scope of traditional hydrogels.

4. Experimental Section

Lauryl acrylate (LA) was purchased from abcr. polypropylene glycol dimethacrylate (PPGDMA), 1-iodooctane, 1-decanol, oil blue n, oil red o, sudan I, and mineral oil (M5904, contains 36 wt% naphthenes and 64 wt% of other saturated paraffins)[45] were purchased from Sigma–Aldrich. Irgacure 379 (2-dimethylamino-2-(4-methyl-benzyl)−1-(4-morpholin-4-yl-phenyl)butan-1-one) was purchased from IGM resins. 1-Octanol, 1-nonanol, toluene, and hexadecane were purchased from Alfa Aesar. n-octane was purchased from Merck. PPGDMA was purified with an Al_2O_3-basic column to remove the inhibitor. Other solvents and reagents were used without further purification.

Ink Preparation: Ink compositions contained 100:0, 80:20, 70:30, or 50:50 weight ratio of LA to mineral oil. After that, in relation to the quantity of monomer, 0.5/0.75/1 mol% of PPGDMA and 4 wt% of initiator irgacure 379 (2-dimethylamino-2-(4-methyl-benzyl)−1-(4-morpholin-4-yl-phenyl)butan-1-one) were added. To achieve the colored printed object shown in Figure 4A, 0.05 wt% of Sudan I was additionally added to the inks. All components were mixed and sonicated for 30 min at 35 °C to completely dissolve the photoinitiator. The ink was stored in a dark flask at 5 °C and equilibrated to room temperature before printing.

Printing Protocol: All objects were printed using a commercial DLP-based 3D printer Miicraft 110 Prime (Taiwan) with the following parameters: wavelength 385 nm, layer thickness 50 µm, curing time per layer 10 s, and power ratio 0.5 (a Miicraft software printing parameter corresponding to 50% of the maximum brightness of light engine).

Swelling: For swelling, printed organogels were sonicated in 30–50 mL of isopropanol for 48 h to remove the sacrificial printing solvent, photo initiator, and unreacted monomer/crosslinker. After that, the objects were dried on air for 8–12 h and were placed in excess of the desired solvent. To measure swelling, the objects were weighed before and after swelling at 24 h intervals, after which the swelling ratios were calculated from the mass of the dried (W_{dr}) and swollen gel (W_{sw}) according to the following formula:

$$\text{Swelling}\,[\%] = (W_{sw} - W_{dr})\, W_{dr}^{-1}\, 100\% \quad (1)$$

Wet and Solid Adhesion: For measuring the liquid and solid adhesion of organogels, sliding angles at a KRÜSS DSA25S Drop Shape Analyzer (Germany) of a 15 µL water drop and 0.91 g neodymium cube, respectively, were recorded. To determine the sliding angle, a 3d-printed organogel with a smooth flat top surface was fixed on a platform. After placing a drop or a cube on the gel, the sample-holding platform started tilting at 1° per second from 0° to 90° with the device camera recording the movement of the sliding object. The angle was determined as the moment the object left its initial position, i.e., starts sliding. For the swollen organogels, prior to the measurement, the excess of swelling liquid was removed by a non-fiber tissue. Each sliding experiment was repeated 5 times. Between the measurements, organogels were re-immersed in their respective solvents to replenish lubrication layers.

Optical Digital Microscopy: Optical digital microscopy images were captured with a VHX-7000 Microscope (Keyence, Japan), 20x lens.

Optical Profilometry: Profiles on the Figure 4B,E were characterized with the optical microscope equipped with the laser VK-X3000 (Keyence, Germany), across the surface of the non-swollen and swollen in mineral oil gel. Axis Y of the profile represents depth, axis X represents the length of sample along which the profile was measured.

Rheology: The tests were conducted on the strain-controlled rheometer ARES G2 (TA Instruments, Eschborn, Germany). For the test, 3 samples were chosen: the non-swollen gel, the gel swollen in n-hexadecane (72 h), and the gel swollen in butyl disulfide (72 h). The test geometry was a 13.0 mm parallel plate, and a constant axial force of 1 N (ca. 11 600 Pa) at an angular frequency $\omega = 1$ rad s^{-1} was applied, while the sample was covered with a solvent trap to prevent solvent evaporation. The fixed value of strain of $\gamma_o = 0.5\%$ was chosen to be in the viscoelastic regime. The low-temperature ramp was carried out over a range of 25 °C to –20 °C for non-swollen and swollen in hexadecane gels, and from 20 to −40 °C for organogel swollen in

dibutyl sulfide. The high-temperature ramp was carried out over a range of 25–100 °C for non-swollen and swollen hexadecane gels. A mobile fume extractor was placed next to the rheometer during all tests to avoid inhalation of any leaking solvent.

Camera: All photos were made with a Canon digital single-lens reflex camera (model: EOS 80D) using a 100 mm macro lens (model: ef 100 mm 1:2.8l macro is usm). Brightness and contrast were adjusted for the images in Figures 2 and 5 for better clarity.

Supporting Information

Supporting Information is available from the Wiley Online Library or from the author.

Acknowledgements

P.A.L. thanks DFG (Heisenbergprofessur; 406232485 and LE 2936/9-1) for the financial support. M.K., N.K.M, and P.A.L. thank the Excellence Cluster "3D Matter Made to Order" (2082/1-390761711) and the Carl Zeiss Foundation for financial support. M. H. would like to thank the Stiftung der deutschen Wirtschaft (sdw) for its support within the framework of the Klaus Murmann Scholarship. N.K.M. was funded by an Internationalisation Fellowship from the Carlsberg Foundation (CF21-0614). Michael Pollard is acknowledged for proofreading as a native speaker.

Open access funding enabled and organized by Projekt DEAL.

Conflict of Interest

The authors declare no conflict of interest.

Data Availability Statement

The data that support the findings of this study are available in the supplementary material of this article, and additional data are available upon request or in RADAR4KIT repository: https://doi.org/10.35097/CGfpUYHmwIjNlbRC.

Keywords

3D-printing, organogels, solvent-tuned properties, stimuli-responsive

Received: February 29, 2024
Revised: April 19, 2024
Published online:

[1] L. Zeng, X. Lin, P. Li, F.-Q. Liu, H. Guo, W.-H. Li, *Prog. Org. Coat.* **2021**, *159*, 106417.
[2] C. L. Esposito, P. Kirilov, V. G. Roullin, *J. Controlled Release* **2018**, *271*, 1.
[3] M. A. Kuzina, D. D. Kartsev, A. V. Stratonovich, P. A. Levkin, *Adv. Funct. Mater.* **2023,**, *33*, 2301421.
[4] Y. Long, B. Jiang, T. Huang, Y. Liu, J. Niu, Z. L. Wang, W. Hu, *Adv. Funct. Mater.* **2023**, *33*, 202304625
[5] J. M. Scheiger, S. Li, M. Brehm, A. Bartschat, P. Theato, P. A. Levkin, *Adv. Funct. Mater.* **2021**, *31*, 2105681.
[6] P. Charoensumran, H. Ajiro, *Polym J* **2018**, *50*, 1021.
[7] Y. Gao, L. Shi, S. Lu, T. Zhu, X. Da, Y. Li, H. Bu, G. Gao, S. Ding, *Chem. Mater.* **2019**, *31*, 3257.
[8] A. Khan, R. R. Kisannagar, S. Mahmood, W.-T. Chuang, M. Katiyar, D. Gupta, H.-C. Lin, *ACS Appl. Mater. Interfaces* **2023**, *15*, 42954.
[9] X. Yu, L. Geng, J. Guo, in *Supramolecular Gels: Materials and Emerging Applications* (Ed.: T. Jiao), Wiley-VCH, Weinheim **2021**, 21.
[10] J.-M. Park, J. Park, Y.-H. Kim, H. Zhou, Y. Lee, S. H. Jo, J. Ma, T.-W. Lee, J.-Y. Sun, *Nat. Commun.* **2020**, *11*, 4638.
[11] F. Mo, Y. Huang, Q. Li, Z. Wang, R. Jiang, W. Gai, C. Zhi, *Adv. Funct. Mater.* **2021**, *31*, 2010830.
[12] J. Lv, X. Yao, Y. Zheng, J. Wang, L. Jiang, *Adv. Mater.* **2017**, *29*, 103032.
[13] G. Chen, S. Liu, Z. Sun, S. Wen, T. Feng, Z. Yue, *Prog. Org. Coat.* **2020**, *144*, 105641.
[14] Z. Li, B. Zhang, S. Jia, M. Ma, J. Hao, *J. Mol. Liq.* **2018**, *250*, 19.
[15] N. L. Smith, A. E. Coukouma, D. C. Wilson, B. Ho, V. Gray, S. A. Asher, *ACS Appl. Mater. Interfaces* **2020**, *12*, 238.
[16] F. Wang, B. Chen, L. Wu, Q. Zhao, L. Zhang, *Cell Rep Phys Sci* **2020**, *1*, 100011.
[17] Z. Wang, M. Heck, W. Yang, M. Wilhelm, P. A. Levkin, *Adv. Funct. Mater.* **2023**.
[18] Y. Jia, G. Sciutto, R. Mazzeo, C. Samorì, M. L. Focarete, S. Prati, C. Gualandi, *ACS Appl. Mater. Interfaces* **2020**, *12*, 39620.
[19] Y. Yu, B. Jin, M. I. Jamil, D. Cheng, Q. Zhang, X. Zhan, F. Chen, *ACS Appl. Mater. Interfaces* **2019**, *11*, 12838.
[20] H. Liu, P. Zhang, M. Liu, S. Wang, L. Jiang, *Adv. Mater.* **2013**, *25*, 4477.
[21] C. Urata, H. Nagashima, B. D. Hatton, A. Hozumi, *ACS Appl. Mater. Interfaces* **2021**, *13*, 28925.
[22] Y. Zhang, Y. Zhao, Z. Peng, B. Yao, Y. Alsaid, M. Hua, D. Wu, Y. Qiu, Q. Pei, X. Zhu, Z. He, X. He, *ACS Mater. Lett.* **2021**, *3*, 1477.
[23] Y. Wang, X. Yao, S. Wu, Q. Li, J. Lv, J. Wang, L. Jiang, *Adv. Mater.* **2017**, *29*, 1700865.
[24] B. Eslami, P. Irajizad, P. Jafari, M. Nazari, A. Masoudi, V. Kashyap, S. Stafslien, H. Ghasemi, *Soft Matter* **2019**, *15*, 6014.
[25] H. Y. Lai, A. d. Leon, K. Pangilinan, R. Advincula, *Prog. Org. Coat.* **2018**, *115*, 122.
[26] X. Yao, J. Ju, S. Yang, J. Wang, L. Jiang, *Adv. Mater.* **2014**, *26*, 1895.
[27] Z. Zhang, L. Wang, H. Yu, F. Zhang, L. Tang, Y. Feng, W. Feng, *ACS Appl. Mater. Interfaces* **2020**, *12*, 15657.
[28] P. Zhang, H. Liu, J. Meng, G. Yang, X. Liu, S. Wang, L. Jiang, *Adv. Mater.* **2014**, *26*, 3131.
[29] J. Oh, D. Baek, T. K. Lee, D. Kang, H. Hwang, E. M. Go, I. Jeon, Y. You, C. Son, D. Kim, M. Whang, K. Nam, M. Jang, J.-H. Park, S. K. Kwak, J. Kim, J. Lee, *Nat. Mater.* **2021**, *20*, 385.
[30] C. Zhao, Q. Lv, W. Wu, *Gels* **2022**, *8*, 297.
[31] K. Ahmed, M. N. I. Shiblee, A. Khosla, L. Nagahara, T. Thundat, H. Furukawa, *J. Electrochem. Soc.* **2020**, *167*, 037563.
[32] Y. Zhang, Y. Zhao, D. Wu, J. Xue, Y. Qiu, M. Liao, Q. Pei, M. S. Goorsky, X. He, *Adv. Mater.* **2019**, *31*, 1902928.
[33] C. S. O'Bryan, T. Bhattacharjee, S. Hart, C. P. Kabb, K. D. Schulze, I. Chilakala, B. S. Sumerlin, W. G. Sawyer, T. E. Angelini, *Sci. Adv.* **2017**, *3*, e1602800.
[34] M. Dong, Y. Han, X. P. Hao, H. C. Yu, J. Yin, M. Du, Q. Zheng, Z. L. Wu, *Adv. Mater.* **2022**, *34*, 2204333.
[35] C. Sun, N. Fang, D. M. Wu, X. Zhang, *Sens. Actuators, A* **2005**, *121*, 113.
[36] Y. Yang, X. Li, X. Zheng, Z. Chen, Q. Zhou, Y. Chen, *Adv. Mater.* **2018**, *30*, 1704912.
[37] F. Horkay, A. M. Hecht, E. Geissler, *J. Chem. Phys.* **1989**, *91*, 2706.
[38] G. Hoti, F. Caldera, C. Cecone, A. Rubin Pedrazzo, A. Anceschi, S. L. Appleton, Y. Khazaei Monfared, F. Trotta, *Materials* **2021**, *14*, 478.
[39] O. Chiantore, L. Trossarelli, M. Lazzari, *Polymer* **2000**, *41*, 1657.
[40] L. Li, J. M. Scheiger, T. Tronser, C. Long, K. Demir, C. L. Wilson, M. A. Kuzina, P. A. Levkin, *Adv. Funct. Mater.* **2019**, *29*, 1902906.
[41] H. Zhang, P. Wang, D. Zhang, *Colloids Surf. A* **2018**, *538*, 140.
[42] G. A. Hurst, M. Bella, C. G. Salzmann, *J. Chem. Educ.* **2015**, *92*, 940.

[43] A. M. Fuentes-Caparrós, Z. Canales-Galarza, M. Barrow, B. Dietrich, J. Läuger, M. Nemeth, E. R. Draper, D. J. Adams, *Biomacromolecules* **2021**, *22*, 1625.
[44] W. M. Haynes, *CRC Handbook of Chem. and Phys.: A Ready-Reference Book of Chemical and Physical Data*, CRC Press, Boca Raton **2014**.
[45] L. Helden, K. Dietrich, C. Bechinger, *Langmuir* **2016**, *32*, 13752.